HAL open science

Uranium solubility and speciation in reductive soda-lime aluminosilicate glass melts

Pierrick Chevreux, Laurent Tissandier, Annabelle Laplace-Ploquin, Tonya Vitova, Sebastian Bahl, Fabienne Le Guyadec, Etienne Deloule

▶ **To cite this version:**

Pierrick Chevreux, Laurent Tissandier, Annabelle Laplace-Ploquin, Tonya Vitova, Sebastian Bahl, et al.. Uranium solubility and speciation in reductive soda-lime aluminosilicate glass melts. Journal of Nuclear Materials, 2021, 544, pp.152666. 10.1016/j.jnucmat.2020.152666 . cea-03104222

HAL Id: cea-03104222

https://cea.hal.science/cea-03104222

Submitted on 8 Jan 2021

HAL is a multi-disciplinary open access archive for the deposit and dissemination of scientific research documents, whether they are published or not. The documents may come from teaching and research institutions in France or abroad, or from public or private research centers.

L'archive ouverte pluridisciplinaire **HAL**, est destinée au dépôt et à la diffusion de documents scientifiques de niveau recherche, publiés ou non, émanant des établissements d'enseignement et de recherche français ou étrangers, des laboratoires publics ou privés.

Distributed under a Creative Commons Attribution - NonCommercial - NoDerivatives 4.0 International License

Journal
Journal of Nuclear Materials

Title
Uranium solubility and speciation in reductive soda-lime aluminosilicate glass melts

Authors
Pierrick Chevreux (a)
Laurent Tissandier (b)
Annabelle Laplace (a)
Tonya Vitova (c)
Sebastian Bahl (c)
Fabienne Le Guyadec (d)
Etienne Deloule (b)

Affiliations
(a) CEA, DES, ISEC, DE2D, Univ. Montpellier, Marcoule, France
(b) Centre de Recherches Pétrographiques et Géochimiques, UMR 7358 CNRS, Université de Lorraine, BP 20, F-54501, Vandoeuvre les Nancy Cedex, France
(c) Institute for Nuclear Waste Disposal, Karlsruhe Institute of Technology, P.O. Box 3640, 76021 Karlsruhe, Germany
(d) CEA, DES, ISEC, DMRC, Univ. Montpellier, Marcoule, France

Highlights

- Uranium solubility has been determined in soda-lime aluminosilicate glasses
- HR-XANES can be used to determine uranium oxidation states in glass
- Uranium solubility in glass melt decreases in the order $U^{VI} > U^{V} > U^{IV}$
- The hexavalent uranium content is a key factor for uranium solubility in glass

Abstract
Uranium solubility in aluminosilicate melts of the Na_2O-CaO-Al_2O_3-SiO_2 system with two different Na/Ca ratios was studied at temperatures of 1250–1400 °C and under various redox conditions. A closed thermochemical reactor was used to control the alkali metal activity (sodium oxide content) and the oxygen fugacity imposing the reducing environment on the glass melt (10^{-5} atm < fO_2 < 10^{-15} atm). The compositions of the quenched glasses were analyzed by scanning electron microscopy and electron probe microanalysis. It appeared that uranium solubility decreased with decreasing oxygen fugacity, elucidating the roles of the different valences of uranium. To account for the respective effects of theses valences, we proposed a method to determine the proportion of each uranium oxidation state in the glass sample. The coexisting U^{VI}, U^{V}, and U^{IV} species have been characterized for the first time in glass samples using U M_4 edge high energy resolution X-ray absorption near-edge structure. Results showed that the lowest solubility values, of approximately 1 mol% UO_2, were obtained under strongly reducing conditions, and thus with U^{IV} as the main valence. Under higher oxygen fugacity, uranium solubility was controlled and drastically enhanced by the U^{VI} concentration in the melt.

Keywords
Uranium, solubility, aluminosilicate glass melt, HR-XANES, oxidation states.

1 Introduction

A good understanding of the behavior of uranium in glass melts is fundamental for the use of aluminosilicate glasses as matrices for nuclear waste. However, the basic chemistry of uranium in glass melts is quite complex. Redox equilibria of U^{VI}-U^{V}-U^{IV} have been established in several glass-forming oxide liquids (mostly silicate) [1-3]. Unlike in aqueous solvents, in which redox processes are mainly ruled by the U^{VI}-U^{IV} couple, the pentavalent state of uranium U^{V} is highly stabilized in glass systems [1, 4, 5]. The specific role of U^{V} is difficult to unravel in solubility studies since, as an intermediate valence state, U^{V} is systematically accompanied, by U^{IV} or U^{VI}, depending on the redox conditions.

It is well-known that the oxidation state of multivalent actinides (for example U, Pu and Np) significantly affects their solubility in a glass matrix [2, 6-8]. Some authors have demonstrated that the oxidized U^{VI} species is much more soluble than the reduced U^{IV} species in glass [1, 2, 9, 10]. When the hexavalent form U^{VI} is significantly predominant, the solubility in silicate glass ranges from 13 to 20 mol% UO_2 for temperatures between 1150 and 1400 °C. Conversely, the solubility drops to between 1 and 5 mol% UO_2, for similar synthesis conditions (temperatures and glass compositions) when the tetravalent U^{IV} species prevails. Although reported data is scarce, the solubility of U^{IV} in aluminosilicate glasses does not exceed 1.2 mol% UO_2 at 1240 °C [1]. In silicate melts, U^{VI} ions occur in the uranyl configuration with two shorter axial U-O bonds (≈ 1.8 Å) and four to six longer equatorial bonds (≈ 2.3 Å) according to extended X-ray absorption fine structure (EXAFS) data [11-15]. The linear structure of the uranyl ion $(UO_2)^{2+}$ likely fits well in the glass structure leading to the high solubility of U^{VI}. Conversely, no real data about the solubility of U^{V} in glass is available in the literature because the pentavalent state of uranium is more often detected in mixtures with U^{VI} and/or U^{IV}. As the three oxidation states can coexist in the glass melt, uranium solubility data must be carefully interpreted and compared. Furthermore, glass-making parameters such as the imposed oxygen fugacity, melting temperature and glass composition have significant impacts on the equilibrium distribution of uranium valence states [1]. Oxidized species are favored first by high oxygen fugacities and then by low temperatures while reduced species are stabilized by low oxygen fugacities and high temperatures. The redox equilibria also shift with the glass composition, with the oxidized state generally favored when the basicity of the melt increases [16, 17]. Thus, it appears that it is necessary to control all parameters of the uranium-doped glass synthesis and to determine the fraction of each uranium valence state in such glasses in order to accurately study uranium solubility in glass melts.

Various studies have characterized uranium oxidation states in glasses using optical absorption spectroscopy [1, 2, 4, 11, 18, 19] and X-ray absorption spectroscopy at the U L_3 edge [11-15, 20-22]. Although some authors have estimated the distribution of each redox state of uranium in glass samples [1, 4, 23], their exact and direct determination remains a key challenge. For example, the U L_3 edge spectra are characterized by broad features due to large core-hole lifetime broadening effects [24] which makes it difficult to accurately determine U^{IV}, U^{V} and U^{VI} species simultaneously present in the same material. Recently, uses of the high energy resolution X-ray absorption near-edge structure (HR-XANES) technique at the U M_4 edge have highlighted the ability of this technique to assess the oxidation state distribution in mixed-valence uranium oxides [25-31]. In this technique, the spectral resolution is high enough to observe a chemical shift of the main absorption peak for each uranium valence state, in particular the transition from U^{IV} to U^{V} [26].

In this study, we have investigated the uranium solubility in two soda-lime aluminosilicate glasses melted under reducing conditions with oxygen fugacities ranging from 10^{-5} atm to 10^{-}

^{15} atm. This aluminosilicate glass matrix was selected for the immobilization of intermediate-level waste (ILW) including actinides such as uranium and plutonium, via an innovative vitrification process as already described in previous work [32]. In this process, the glass melt is in contact with molten metals at high temperatures (1250–1400 °C), imposing highly reducing conditions under which uranium solubility has to be assessed. In this study, in order to limit the volatilization of sodium that can occur under reducing environments [33, 34], a thermochemical reactor was used to control both oxygen fugacity and the chemical composition of the silicate melt [35-38]. We also herein present a convenient and effective method for determining the distribution of the oxidation states of uranium in glass samples by HR-XANES at the U M_4 edge. The results are discussed under the framework of uranium solubility in glass melts.

2 Experimental

2.1 Glass making

A set of glasses were synthetized in this work. First, two batches of U-free starting glasses were elaborated, and then some aliquots were doped with high concentrations of uranium to test its solubility. Besides these syntheses, larger crystal-free U-doped glass samples were also prepared to allow XANES characterization.

2.1.1 Starting glasses

Two U-free starting aluminosilicate glasses were prepared with high purity component oxides and carbonates following previously described protocol [32]. The chemistry and homogeneity of glasses (herein named A and B) were assessed by energy and wavelength dispersive spectroscopy (EDS and WDS) analyses (Table 1). Glass B was obtained from glass A by replacing all Na_2O with CaO. These glasses were subsequently milled and the particle size of the powder was less than 200 µm.

For elaboration of the uranium-doped glass, UO_2 powder was added to each ground starting glass using an agate mortar for homogenization. The uranium powder, sourced from CEA stock, was a mixture of UO_2 (> 90 %) and U_3O_8, and was composed of agglomerates ranging in size from 10 µm to 40 µm, also containing submicron-sized grains.

Glass composition (mol%)						
Sample name	SiO_2	Al_2O_3	CaO	Na_2O	UO_2	Nd_2O_3
A (*)	58.64 ± 0.12	6.94 ± 0.04	14.10 ± 0.12	20.32 ± 0.08	0	0
B (*)	57.08 ± 0.13	6.45 ± 0.12	36.45 ± 0.14	0	0	0
ANd1	57.85 ± 0.14	6.61 ± 0.03	14.20 ± 0.04	20.51 ± 0.11	0	0.83 ± 0.01
AU4	55.48 ± 0.37	6.19 ± 0.08	13.25 ± 0.11	20.88 ± 0.39	4.21 ± 0.29	0
BU4	54.27 ± 0.07	6.02 ± 0.12	36.23 ± 0.19	0	3.48 ± 0.05	0

Table 1: Glass compositions (mol%) of U-free and U-doped glasses determined by EDS or WDS analyses. (*) denotes samples analyzed by WDS. UO_2 was replaced with Nd_2O_3 in the ANd1 glass used as sodium reservoir for the thermochemical cell.

2.1.2 U-doped glasses for solubility measurements

The strategy developed involved the elaboration of uranium-doped glasses under oxidizing conditions as a first step, and the imposition of reducing conditions on the glass melt as a second step. Oxidizing conditions enable the largest amount of uranium to be incorporated into the glass matrix structure [1, 5, 39].

Uranium was thus incorporated in excess, relative to uranium solubility limits expected in reductive melts. Approximately 500 mg of a mixture containing approximately 4 mol% UO_2 in the powder of glass A and B was melted at 1400 °C for 18–22 h in a platinum crucible (Ø = 10 mm, h = 10 mm) under air. Then, the crucible was removed from the furnace and quenched in air. Optically the obtained glasses, AU4 and BU4, appear completely transparent, and chips of these glasses were analyzed (Table 1). No crystallization was detected by scanning electron microscopy (SEM) and uranium concentration (SEM-EDS analyses) was homogeneous within each sample. The AU4 and BU4 glasses were subsequently ground and used for the second step of the protocol. These synthetic conditions thus ensured that, for each composition, uranium was uniformly distributed in all the samples used in this study.

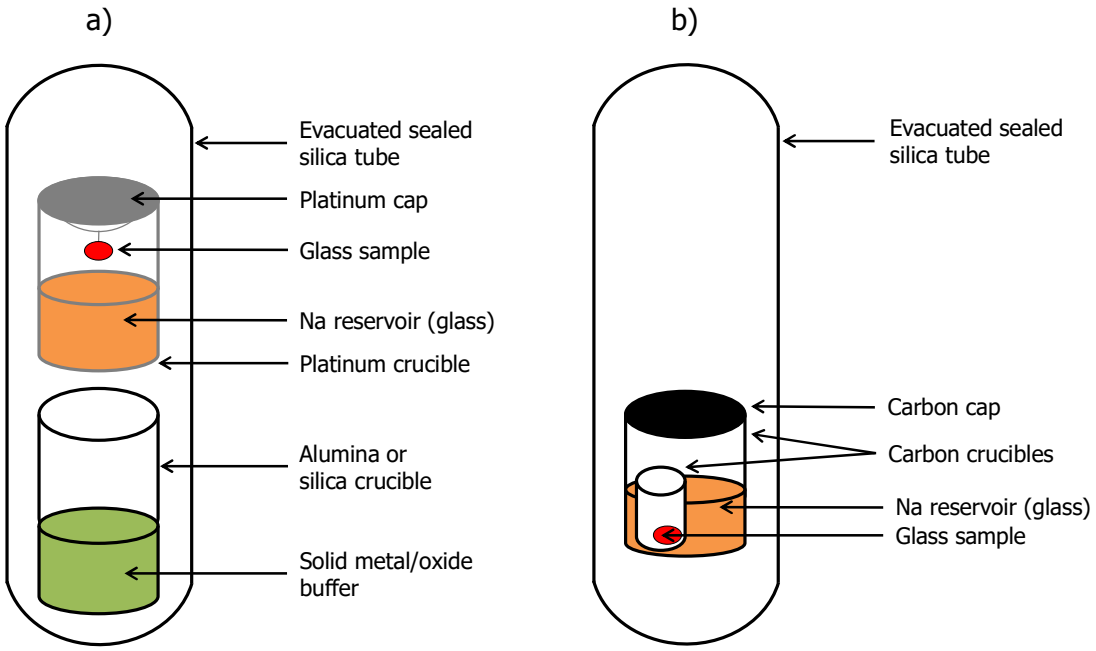

Fig. 1. Schematic illustration of the thermochemical cells used for uranium solubility experiments in alkali-rich aluminosilicate glasses. The oxygen fugacity was imposed by (a) the solid metal/oxide buffers or by (b) the carbon crucible.

The second step consisted of imposing redox conditions on tiny U-doped glass samples with a specific experimental procedure to reach equilibrium quickly. Samples were glass beads of a few millimeters obtained using the Pt wire loop technique [40, 41]. Approximatively 30 mg of former U-doped glass powder mixed with polyvinyl alcohol as a binder were preheated in a muffle furnace at 1400 °C in air for 1 min.

For the Na-free glasses, experiments were carried out in a tubular furnace at 1400 °C for 24 h. The glass beads were fixed to an alumina stick or placed in a carbon crucible (Ø = 10 mm, h = 10 mm) and then introduced directly at high temperature in the furnace. The oxygen fugacity was controlled by calibrated CO_2/CO gas mixtures or imposed by sealing sample under an argon atmosphere in a carbon crucible closed with a carbon lid (Table 2). In the latter case, no need to mix the powder with a binder, the sample directly formed a glass ball due to high surface tension between the carbon crucible and melt. After the run, the glass sample was quenched in air to prevent crystallization during cooling.

For the Na-rich glasses, a thermochemical cell was used in order to avoid loss of Na_2O via volatilization [36, 37]. This closed system allows independent control of alkali activity in the silicate melt, oxygen fugacity and temperature. The cell was composed of an evacuated silica tube ($Ø_{ext}$ = 22 mm, $Ø_{int}$ = 18 mm, h = 100 mm) containing the glass sample, a Na reservoir and an oxygen buffer (Fig. 1) and sealed under primary vacuum ($P \approx 10^{-2}$ mbar). Two experimental assemblies were employed in this work. In the first setup, the glass sample was suspended from a Pt lid in the Pt crucible (Ø = 16 mm, h = 20 mm) containing the Na reservoir (Fig. 1a). The Pt crucible was placed on top of the crucible containing the buffer. The oxygen fugacity was controlled by a metal/oxide solid buffer such as Ni/NiO or Fe/FeO (Table 2). The buffers were introduced in a silica or alumina crucible to prevent them from reacting with the cell and the Pt crucible. In the second assembly (Fig. 1b), a carbon crucible (Ø = 18 mm, h = 20 mm) shut with a carbon lid was used to reach very low oxygen fugacity ($fO_2 < 10^{-12}$ atm). The crucible contained the Na reservoir and a smaller carbon crucible (Ø = 10 mm, h = 10 mm)

containing the glass sample. In both systems, the Na vapor partial pressure was imposed by the so-called Na reservoir, which is composed of approximatively 3.5 g of U-free glass melt with a composition similar to those glass samples (Table 1). For practical reasons, uranium was replaced with neodymium as a surrogate for uranium in this ANd1 glass containing almost 1 %mol Nd_2O_3. The quantity of ANd1 glass was sufficient to ensure that its Na_2O concentration remained roughly constant after the experiment. Assuming that the sodium activities in the molten sample and in the Na reservoir must be equal at thermodynamic equilibrium, sodium volatilization in the glass sample should be strongly limited within the reactor. Once prepared, the thermochemical cell was introduced into a muffle furnace at 1250 or 1400 °C, on an alumina support to keep the system in the vertical alignment. The duration of each run was about 60–80 h, to ensure that all components inside the cell were well-equilibrated [37]. The silica tube was then removed from the furnace and quenched in air.

In order to confirm that oxygen fugacity and sodium oxide activity were accurately imposed to the glass samples, the presence of both the metal and oxide phases in the solid buffers, and the sodium content in the reservoir were systematically checked after each run.

Samples are named as following: AU4-IW2, for instance. The first part (before hyphen) refers to the glass used and the second part (after hyphen) indicates the redox and temperature conditions imposed to the glass sample. NNO, IW and C correspond to Ni/NiO, Fe/FeO and carbon buffers (or gas mixture), respectively. The digit 2 corresponds to a temperature of 1400 °C (none means 1250 °C).

	fO_2 (atm)				
Temperature	Buffers			Gas mixture (vol%)	
	Ni/NiO	Fe/FeO	Carbon	2.8% CO 97.2% CO_2	78.3% CO 21.2% CO_2
1250 °C	$10^{-7.1}$	$10^{-11.3}$	10^{-15}	/	/
1400 °C	$10^{-5.8}$	$10^{-9.7}$	10^{-13}	$10^{-5.6}$	$10^{-9.7}$

Table 2: Oxygen fugacities imposed by buffers or gas mixture at several temperatures.

2.1.3 U-doped glasses for XANES measurements

For XANES analyses, three glasses containing 1.5 mol% UO_2 were prepared from glass A. The mixtures, each approximately 80 mg of powder, were melted at 1250 °C for several hours (between 3 and 6 h) under different redox conditions and then quickly cooled by shutting off the furnace. The AU-Ox and AU-Ar glasses were elaborated in a Pt crucible (Ø = 8 mm, h = 5 mm) under air ($fO_2 = 10^{-0.7}$ atm) and argon atmospheres ($fO_2 \approx 10^{-6}$ atm), respectively. The buffered oxygen fugacity using an Ar flux was estimated from the purity of the gas (99.9999% with oxygen considered as the main impurity). These glass samples were completely homogenous as confirmed by SEM-EDS analyses. The AU-C glass was fused in a carbon-based crucible under Ar atmosphere ($fO_2 = 10^{-15}$ atm, evaluated by in-situ measurements; see section 2.2.3). Uranium was not fully dissolved in the AU-C glass melt, and clusters of U-bearing crystals were observed at the bottom. Therefore, a small upper part of the AU-C glass that did not exhibit any observable crystallization was considered exclusively in this work. This revealed some difficulties in incorporating UO_2 into the glass melt under a strongly reducing environment, and supports our strategy of performing solubility experiments

on glass samples previously prepared under oxidizing conditions (see section 2.1.2). The surfaces of the samples prepared for these analyses had an area of at least 6 mm^2.

2.2 Glass characterization

2.2.1 Solubility measurements

The uranium solubility was defined in this study as the maximum UO_2 concentration that can be loaded in the glass matrix. The achievement of equilibrium was attested by the fact that no uranium concentration gradients were observed in the U-saturated glasses. As an excess of uranium was introduced in the experimental procedure, U-bearing crystals should be present in equilibrium with the vitreous phase.

Quenched glass samples were mounted in epoxy resin, polished, and carbon-coated before characterization. Glass and crystal compositions were determined using electron microprobe with wavelength dispersive X-ray spectroscopy (WDS; CAMECA-SX 100) or scanning electron microscopy (SEM; JEOL-JSM 6510) coupled with energy dispersive X-ray spectroscopy (EDS). The conditions for WDS analyses were an acceleration voltage of 15 kV, a beam intensity of 12 nA, and the utilization of standards. The counting times for peaks and the background were 10 s and 5 s respectively for Na, Ca, Si, Al, U and Nd. All analyses were performed from the core to the rim of each sample using a medium magnification to limit Na migration during the acquisition (~100 μm^2). The composition of each glass was determined as the normalized mean of 6 to 40 individual analyses. Total solubilized uranium content is expressed as the mole percent of UO_2 (mol% UO_2). The random uncertainty was calculated by multiplying the standard deviation of the mean with the Student's t-factor corresponding to the 95% confidence level. All SEM micrographs shown herein were taken in back-scattered electron (BSE) mode.

2.2.2 Uranium M_4 edge HR-XANES measurements

Glass samples used for the XANES experiments were polished and attached to a dedicated support before characterization. XANES measurements were carried out at the INE-Beamline of the Karlsruhe Research Accelerator (KARA) synchrotron facility (Karlsruhe Institute of Technology, Germany) under dedicated operating conditions (2.5 GeV, 120–150 mA). The beam spot size was estimated to be 500 µm both vertically and horizontally.

The U M_4 edge (3728 eV) incident energy was selected using the (111) reflection from a double Si crystal monochromator. HR-XANES spectra were measured using an X-ray emission spectrometer equipped with five Si (220) crystal analyzers and a silicon drift detector (KETEK) [42]. The HR-XANES spectra at the U M_4 edge were obtained by recording the maximum intensity of the U Mβ emission line (≈3338 eV) as a function of the incident energy. The sample, crystal and detector were positioned on a vertical circle (Rowland geometry) with a diameter of 1 m, which is equivalent to the bending radius of the crystals. The spectrometer was placed in a gastight box wherein a constant He atmosphere was maintained to avoid intensity losses due to scattering and absorption of low energy M*β* fluorescence photons by air. The measured spectra did not exhibit evidence of radiation damage. Several spectra, at least three, were collected for each sample to improve the counting statistics. The intensity was normalized to the incident flux. A combined (incident convoluted with emitted) energy resolution was experimentally evaluated at 1 eV by measuring the full width at half maximum of the quasi-elastic peak. All experiments were performed at room temperature. The position of the white-line maximum was determined from the first zero-crossing of the first derivative. PyMca

software was used to remove the background and normalize the spectra [43]. Linear combination fitting (LCF) was done using ATHENA software [44]. The goodness of fit value is represented by the R factor defined as following :

$$R = \frac{\sum(data-fit)^2}{\sum(data-fit)} \quad \textbf{Eq. 1}$$

This equation indicates that the lower the R factor, the better fit.

2.2.3 Oxygen fugacity in situ measurements

The oxygen fugacity imposed by the carbon-based crucible was evaluated by in-situ measurements of the oxygen fugacity in a glass melt using an electrochemical technique. An oxygen sensor [45] composed of two electrodes, namely an iridium wire as a working electrode and a Ni/NiO reference electrode contained in a magnesia stabilized zirconia closed sheath ($pO_{2\ reference}$) was immersed in the melted glass and linked to a potentiostat. At zero current, a potential difference (ΔE, in V) measured between the electrodes, is related to the oxygen fugacity in the melt ($fO_{2\ melt}$) according to the following equation [46]:

$$\Delta E = \frac{RT}{4F} ln \frac{fO_{2\,melt}}{pO_{2\,reference}} \quad \textbf{Eq. 2}$$

where R, Boltzmann constant ($J.mol^{-1}.K^{-1}$)
T, temperature (K)
F, Faraday constant ($C.mol^{-1}$)
$pO_{2\,reference}$, known value (atm)

These electrochemical experiments were performed at temperatures from 1250 to 1400 °C using a surrogate glass with a composition close to that of glass A. Approximatively 150–200 g of this glass were preheated in a carbon-based crucible at 1400 °C for 10 h, cooled at room temperature and then introduced into an alumina crucible and the system was placed in the furnace dedicated for electrochemical measurements. The measured values of oxygen fugacity were approximate ($fO_2 = 10^{-15}$ atm at 1250 °C and $fO_2 = 10^{-13}$ atm at 1400 °C).

3 Results

3.1 Uranium solubility study

Sample name	Temperature (°C)	fO_2 (atm)	SiO_2 (mol%)	Al_2O_3 (mol%)	CaO (mol%)	Na_2O (mol%)	UO_2 (mol%)	MgO (mol%)
AU4-NNO	1250	$10^{-7.1}$	63.20 ± 0.23	6.69 ± 0.07	8.95 ± 0.25	16.60 ± 0.30	2.28 ± 0.10	2.28 ± 0.06
AU4-IW	1250	$10^{-11.3}$	59.96 ± 0.28	6.53 ± 0.04	13.13 ± 0.06	16.87 ± 0.26	1.24 ± 0.03	2.27 ± 0.03
AU4-C	1250	10^{-15}	65.69 ± 0.35	6.87 ± 0.05	9.27 ± 0.11	14.78 ± 0.28	1.02 ± 0.04	2.37 ± 0.08
AU4-NNO2	1400	$10^{-5.8}$	59.30 ± 0.24	6.44 ± 0.08	13.10 ± 0.17	16.80 ± 0.19	2.08 ± 0.03	2.28 ± 0.11
AU4-IW2	1400	$10^{-9.7}$	61.11 ± 0.56	6.51 ± 0.04	14.13 ± 0.33	14.26 ± 0.93	1.88 ± 0.07	2.11 ± 0.05

AU4-C2 (*)	1400	10^{-13}	64.28 ± 0.28	7.34 ± 0.07	14.75 ± 0.39	9.67 ± 0.14	1.48 ± 0.02	2.48 ± 0.06
BU4-NNO2	1400	$10^{-5.6}$	55.03 ± 0.08	6.04 ± 0.08	36.08 ± 0.08	0	2.85 ± 0.02	0
BU4-IW2	1400	$10^{-9.7}$	55.77 ± 0.25	6.11 ± 0.03	36.26 ± 0.24	0	1.93 ± 0.05	0
BU4-C2	1400	10^{-13}	54.04 ± 0.24	6.40 ± 0.07	37.86 ± 0.25	0	1.70 ± 0.05	0

Table 3. Glass compositions (mol%) of equilibrated U-doped glass samples at the specified temperature and under a given oxygen fugacity. Glass samples were analyzed by WDS. (*) indicates that the sample was not well-equilibrated (unclosed thermochemical cell).

In this work, uranium solubility in aluminosilicate melts was studied as a function of the imposed oxygen fugacity (10^{-15} atm < fO_2 < 10^{-5} atm), melting temperature and glass composition (1250 and 1400 °C for glass A and 1400 °C for glass B).

Uranium solubility was determined by measuring the uranium dioxide concentration in the U-saturated glasses in equilibrium with U-bearing crystals. The glass compositions measured by WDS are given in Table 3. In addition to the presence of U-bearing crystals, the absence of uranium concentration gradient means that the equilibrium state was approached in our glass samples (Fig. 2).

After checking the buffers and the Na reservoir concentrations from our experimental set-ups, it appeared that all but one of the solubility experiments were successful. Sodium volatilization was efficiently limited except for the AU4-C2 sample. Indeed, a hole appeared in the cell containing the AU4-C2 sample, and it was thus quenched after 7 hours. Analyses show that sodium is rapidly lost (Table 3) in such an “unclosed” system, in part motivating the specific experimental design we used. Consequently, the uranium concentration in the AU4-C2 sample in which the equilibrium state was not reached, must be interpreted carefully. It should also be noted that the Na-rich samples were contaminated with magnesium (around 2 mol% MgO) which likely occurred during the grinding step, exacerbated by the use of small quantities. Changes in calcium oxide concentrations will be explained in the following section.

The total solubilized uranium content in the melt is plotted as a function of the imposed oxygen fugacity for different glass compositions and temperatures (Fig. 3). The general trends are the same for both compositions, with uranium solubility decreasing when oxygen fugacity is reduced. Under an oxygen fugacity of between 10^{-15} atm and 10^{-5} atm, the solubility ranges from 1 to 3 mol% UO_2, and seems to increase with increasing temperature. Under intermediate oxygen fugacity conditions ($fO_2 = 10^{-6}$ atm), the Na-free glass B incorporates at 1400 °C more uranium than the A glass but both melts have comparable solubility limits under lower oxygen fugacity conditions. Note that uranium solubility limits were not determined in the glass samples elaborated under an air atmosphere ($fO_2 = 10^{-0.7}$ atm). Since uranium saturation was not reached, the solubility in the melt should be greater than or equal to the incorporated uranium content (> 3.5 mol% UO_2).

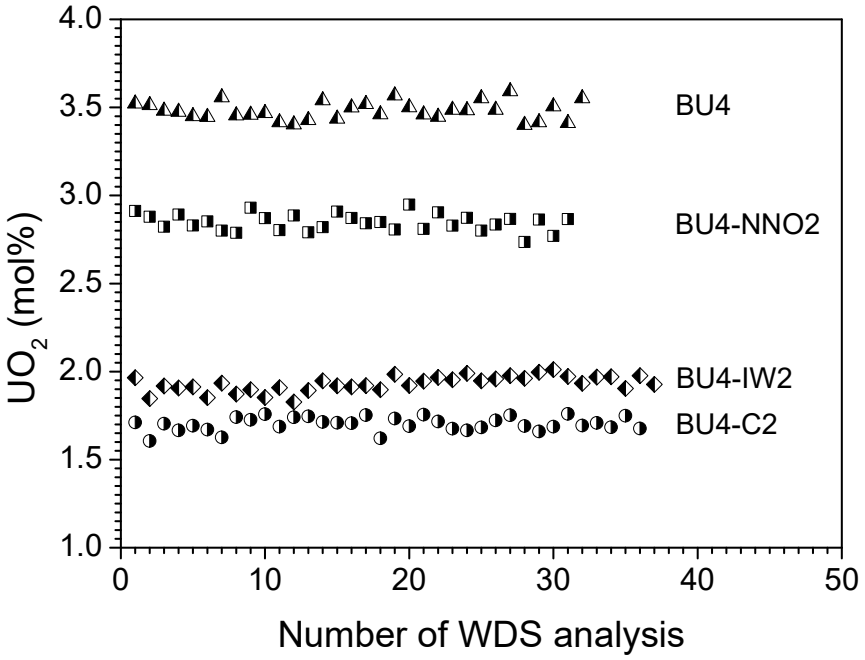

Fig. 2. Total uranium contents measured by WDS analysis in glass B samples elaborated under various redox conditions.

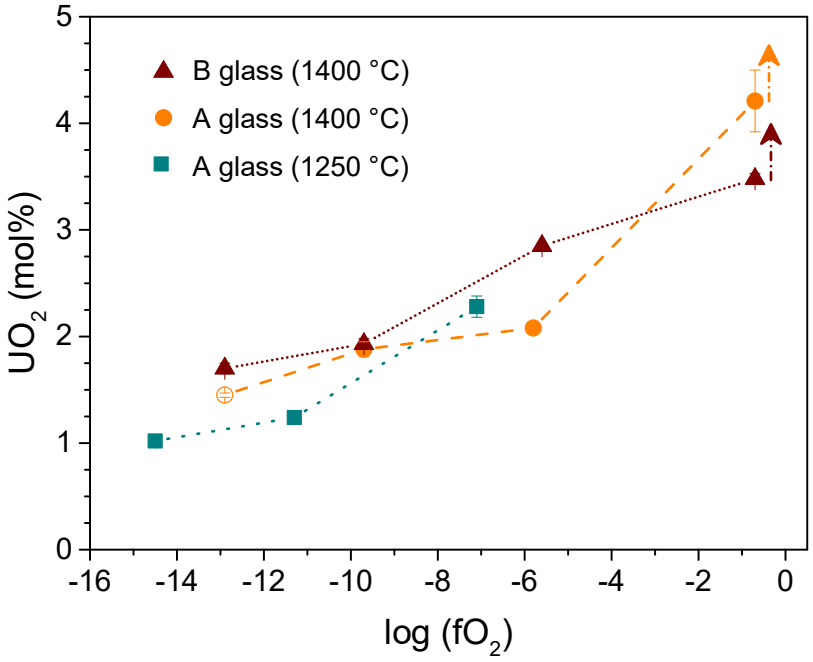

Fig. 3. Total uranium contents reported as a function of the oxygen fugacity for different glass compositions and temperatures. The full symbols represent solubility limits of uranium in glass melts while the open symbol represents uranium concentration for the

glass sample that was not equilibrated. The arrows indicate that the maximal amount of uranium incorporated into the glass matrix is not reached. The random uncertainties are represented by error bars.

Fig. 4 shows typical quenched glass samples. As expected, UO_2 crystals around the vitreous phase were observed by SEM and exhibit two different morphologies. The exact stoichiometry of these crystals was not determined in this work. The first type consists of isometric and euhedral crystals ranging in size from 1 µm to 15 µm, which are mainly located at the bottom of the glass sample and around the Pt wire (Fig. 4 a and b). These particles seem to sediment under gravity over the course of the experiments. The second type is characterized by crystals with a dendritic shape (Fig. 4 c and d) that are larger (up to 200 µm) and dispersed though the entire glass sample. These Y-shaped crystals are only observed at 1250 °C and under highly reducing conditions ($fO_2 < 10^{-10}$ atm). The amount of U-bearing crystals seems to increase with decreasing oxygen fugacity. In the surroundings of both types of uranium oxide crystals, no significant variations in glass composition is detected. EDS/WDS analyses reveal that the UO_2 crystals contain some impurities such as calcium (up to 9 mol% CaO). The incorporation of calcium into the crystalline structure is in good agreement with the UO_2-CaO binary phase diagram [47], and may explain variations in the amount of CaO in some glass samples.

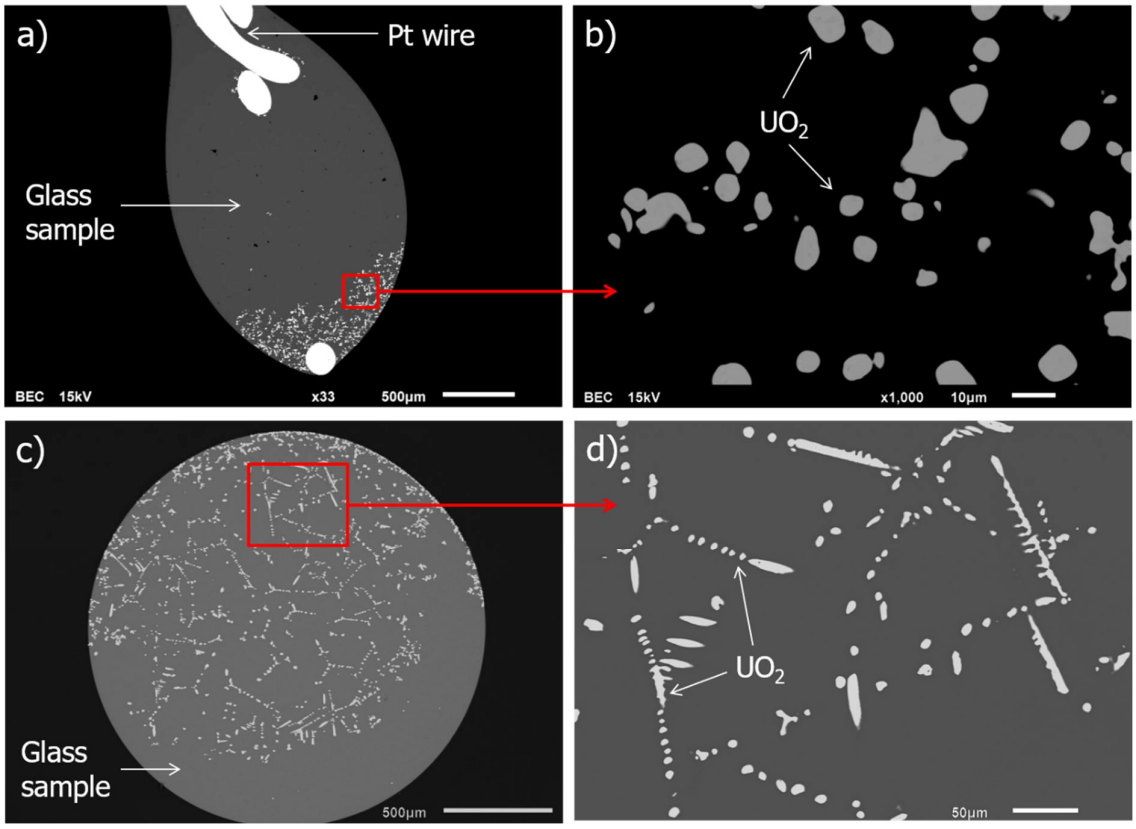

Fig. 4. SEM images of (a, b) BU4-NNO2 and (c, d) AU4-C glass samples showing the typical heterogeneities after the solubility experiments, at 1400 and 1250°C, respectively.

3.2 X-ray absorption near edge structure (XANES) study

U M_4 edge HR-XANES measurements were performed in order to determine the distribution of the U oxidation states in the glass samples. Three uranium-doped soda-lime aluminosilicate

glasses, namely AU-Ox ($fO_2 = 10^{-0.7}$ atm), AU-Ar ($fO_2 = 10^{-6}$ atm), and AU-C ($fO_2 = 10^{-15}$ atm), were elaborated under oxidizing, intermediate, and strongly reducing conditions, respectively.

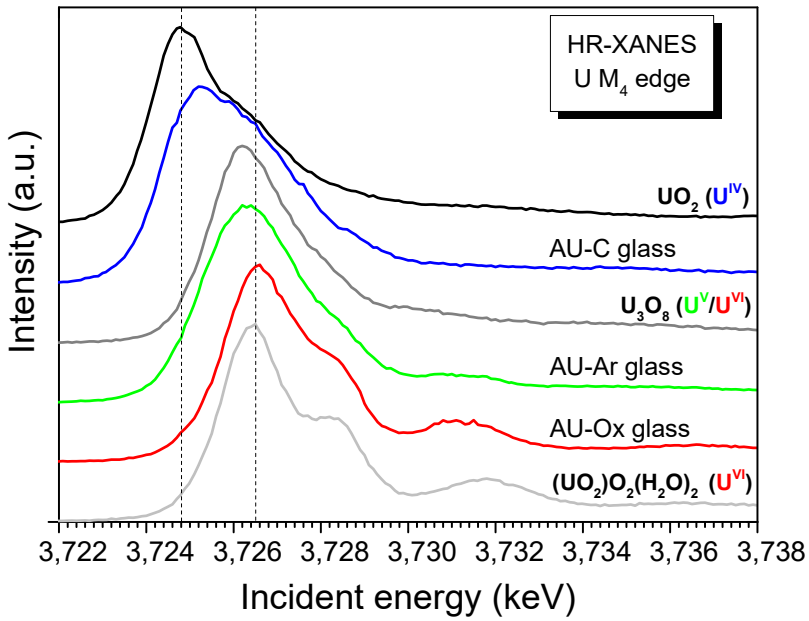

Fig. 5. HR-XANES spectra of the U-doped glasses (AU-Ox, AU-Ar, and AU-C samples) measured at the U M_4 edge and compared with the reference spectra of UO_2, U_3O_8 and $(UO_2)O_2(H_2O)_2$.

The HR-XANES spectra of the U-doped glasses were collected at the U M4 edge, along with spectra of UO_2, U_3O_8, and metastudtite $(UO_2)O_2(H_2O)_2$ which were used as reference systems. UO_2 and $(UO_2)O_2(H_2O)_2$ correspond to pure valence, U^{IV} and U^{VI} respectively, and U_3O_8 is a mixed-valence uranium oxide containing 33% U^{VI} and 67% U^{V} [26, 30]. In Fig. 5, the glass absorption spectra recorded are compared with reference spectra. Each absorption spectrum is characterized by a strong resonance which is referred to as the white line (WL). When moving an oxidation state of U^{IV} to U^{VI}, a chemical shift of the WL to a higher energy is expected. Some additional and less-intense resonances can also be observed at higher energies. The energies (positions) of the main resonances for the glass samples and reference materials are summarized in Table 4. The obtained spectral features and resonance positions of the reference compounds are representative of those described in previous work [25-31, 48, 49].

Compound	White line peak (eV)	Second resonance (eV)	Third resonance (eV)	Ref
$U^{+IV}O_2$	3724.8	/	/	This study
$U^{+IV}O_2$	3725.2	/	/	[30]
$U^{+IV}O_2$	3725.3	/	/	[25]
$U^{+IV}O_2$	3725.1	/	/	[26]
$U^{+IV}O_2$	3724.5	/	/	[29]
$U^{+IV}O_2$	3725.2	/	/	[28]
$U^{+IV}O_2$	3725.2	/	/	[27]
$U^{+IV/+V}{}_4O_9$	3725.3	3726.4	/	[27]
$KU^{+V}O_3$	3276.3	/	/	[27]
$U^{+V/+VI}{}_3O_8$	3726.2	/	/	This study
$U^{+V/+VI}{}_3O_8$	3726.4	/	/	[30]
$U^{+V/+VI}{}_3O_8$	3726.4	/	/	[25]
$U^{+V/+VI}{}_3O_8$	3726.2	/	/	[26]
$U^{+V/+VI}{}_3O_8$	3726.2	/	/	[29]
$U^{+V/+VI}{}_3O_8$	3726.8	/	/	[27]
$(U^{+VI}O_2)O_2(H_2O)_2$	3726.5	3728.4	3731.6	This study
$U^{+VI}O3$	3726.8	3728.6	3732.1	[30]
$U^{+VI}O3$	3726.9	3728.6	/	[25]
$U^{+VI}O3$	3726.8	3728.3	/	[27]
$U^{+VI}O_2(C_5H_8O_2)_2$	3726.9	3729.0	3732.6	[26]
$(U^{+VI}O_2)O_2(H_2O)_2$	3726.6	3728.7	3732.1	[31]
$Cs_2U^{+VI}O_2Cl_4$	3726.4	3728.6	3732.4	[49]
U^{+VI} compounds	~ 3727	~ 3729	~ 3732	[48]

AU-Ox glass	3726.6	3728.4	3731.0	This study
AU-Ar glass	3726.3	/	/	This study
AU-C glass	3725.3	/	/	This study

Table 4: U M_4 edge main resonance energies as measured by HR-XANES, alongside data reported in the literature for comparison.

The HR-XANES spectrum of the AU-Ox glass elaborated under an air atmosphere shows an intense peak at 3726.6 eV, which is very close to the WL of $(UO_2)O_2(H_2O)_2$. Additional resonances, specifically a shoulder and a broad peak, are observed at approximatively 3728.4 eV and 3731.0 eV, respectively, and are attributed to the uranyl ion [26, 49, 50]. The uranyl group consists of two shorter axial U-O bonds (1.8 Å) and four to six longer equatorial U-O bonds (2.3 Å). The position and width of these features in the spectra can vary slightly due to differences in the local environment of the U atoms in the glass sample and in metastudtite. Overall, this leads to the conclusion that the main U valence state in the AU-Ox glass is U^{VI}, although the presence of a very small amount of U^{V} cannot be entirely excluded.
The HR-XANES spectrum of the AU-Ar glass elaborated under an argon atmosphere consists of a WL at 3726.3 eV, a slight shoulder at around 3728.4 eV, and a second broad peak at 3731.0 eV. This spectrum is clearly similar in appearance to the spectrum of U_3O_8. The features specific to the uranyl ion (the second and third resonances), which are absent in the spectrum of U_3O_8, are nevertheless observed in the spectrum of the AU-Ar glass sample. Further, a small amount of U^{IV} may have been present in the glass sample as suggested by the broad main peak. As a consequence, the AU-Ar sample likely contains all U oxidation states, with a significant fraction of U^{V}.
The HR-XANES spectrum of the AU-C glass melted in a carbon-based crucible exhibits the shortest chemical shift of the WL relative to that of UO_2 (only 0.5 eV), which contains U^{IV}. The asymmetric peak of the WL suggests that the main U valence state in the AU-C glass is U^{IV}, accompanied by U^{V}, no U^{VI} species in the uranyl configuration are detected.

The U^{VI}, U^{V} and U^{IV} fractions in the glass samples were subsequently determined by fitting the experimental data with a linear combination of the HR-XANES reference spectra. Linear combination fitting (LCF) using UO_2, U_3O_8, and $(UO_2)O_2(H_2O)_2$ over a -20 to 20 eV energy range around the edge energy gives the relative weights of the reference systems. As reference materials are well-known compounds, the fraction of each U oxidation state in the glass samples can then be deduced. The results corresponding to the best fit obtained for each glass are provided in Table 5, and are consistent with the qualitative analyses of glasses by the XANES spectra. The AU-Ox glass sample exclusively contains 100% U^{VI}. The fits yield 32% U^{VI}, 57% U^{V}, and 11% U^{IV} for the AU-Ar sample and 9% U^{VI}, 17% U^{V} and 74% U^{IV} for the AU-C sample. We are aware that the distributions of the uranium redox states determined by this method are quite approximate. The estimated uncertainty is about 10% for each uranium valence state. A more precise quantitative analysis could be performed using other reference systems, like U_4O_9 [26, 27, 30] as a mixed U^{V}/U^{IV} compound or KUO_3 [27] as a pure U^{V} reference.

Combining the comparison of HR-XANES spectra with those of well-known uranium compounds and the LCF using these reference compounds provides a practical estimation of

the U oxidation state distribution in the AU glasses melted at 1250 °C over a wide oxygen fugacity range. These data will be useful for improving the understanding of uranium solubility in glass melts.

Sample name	Melting conditions			Uranium oxidation state (% vs U total, ± 10%)				
	Crucible	Atmosphere	fO_2 (atm)	U^{VI}	U^{V}	U^{IV}	References used	R factor
AU-Ox	Pt	Air	$10^{-0.7}$	100	0	0	$(UO_2)O_2(H_2O)_2$, U_3O_8	0.019
AU-Ar	Pt	Ar	10^{-6}	32	57	11	$(UO_2)O_2(H_2O)_2$ U_3O_8, UO_2	0.008
AU-C	C-based	Ar	10^{-15}	9	17	74	U_3O_8, UO_2	0.011

Table 5 : Distribution of uranium oxidation states determined by linear combination fitting of HR-XANES spectra, in soda-lime aluminosilicate glasses containing 1.5 mol% UO_2 melted at 1250 °C under different redox conditions.

4 Discussion

4.1 Solubility experiments

XANES results showed that the uranium redox equilibria changed according to the imposed oxygen fugacity. When oxygen fugacity was decreased, the U^{VI} species, initially present in significant proportion in the starting glasses, were progressively reduced to U^{V} and then U^{IV} species. Knowing that reduced forms of uranium are less soluble than the hexavalent form, the glass melt would become supersaturated with uranium, leading to the precipitation of U-bearing crystals. In order to reduce and eliminate supersaturation, the UO_2 crystallization proceeded until equilibrium was reached between the crystal and the melt, leading to the appearance of the euhedral crystals (Fig. 4 and Fig. 6), and thereby locally decreasing the U supersaturation. The crystallization of these particles occurs more readily at the atmosphere/melt and Pt/melt interfaces via a heterogeneous nucleation process [51], and diffusion prevents this supersaturation in the whole sample. For lower temperature experiments (1250 °C), this diffusion did not occur quickly enough to affect the core of the glass bead. Consequently, as the nucleation was more difficult at the core of the glass bead than on the edge of the sample, a higher supersaturation of uranium could be reached, which caused the appearance of dendritic crystals along one or two preferential axes, which is energetically more favorable. The sizes and shapes of all of the observed uranium crystals suggest later growth by an Oswald ripening process [52, 53] during the equilibration time. Note that the stoichiometry of the uranium-bearing crystals (not determined in this study) observed above the solubility limit is likely to provide additional insight into the crystallization mechanisms.

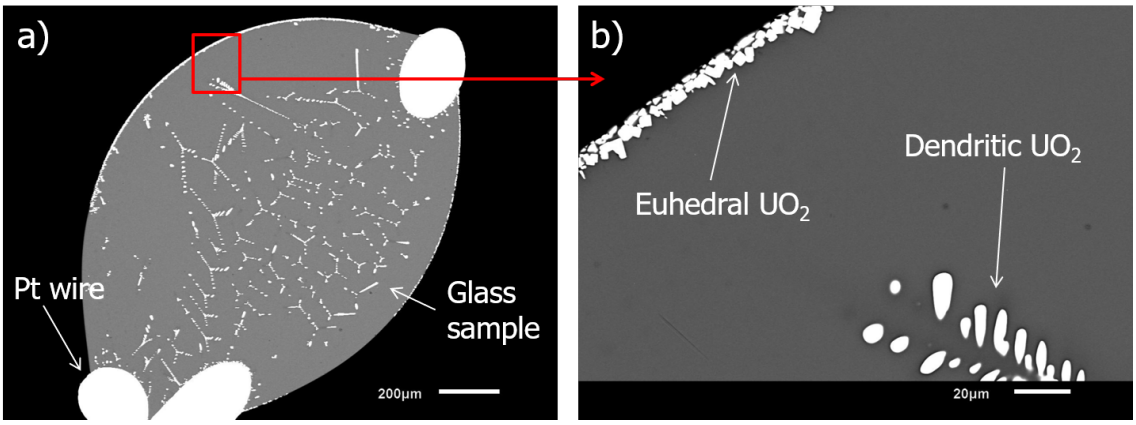

Fig. 6. SEM images of (a, b) AU4-IW glass sample containing two morphological types of uranium crystals (1250 °C).

4.2 Variations in uranium solubility

Considering that the redox states of uranium modify the solubility of uranium in glass, the U oxidation state distribution obtained by HR-XANES is helpful for understanding our solubility data. We thus propose a discussion of the effects of oxygen fugacity, temperature, and glass composition on uranium solubility. All data are summarized in Fig. 3 (solubility) and Table 5 (oxidation states).

Regardless of the melting temperature and glass composition, uranium solubility in the glass melt decreases with decreases in the oxygen fugacity. This assumes that uranium solubility in silicate melts decreases in the order $U^{VI} > U^{V} > U^{IV}$. Indeed, decreasing the oxygen fugacity leads to the reduction of uranium in the glass and each U oxidation state is predominant for a given oxygen fugacity according to our XANES results (Table 5). However, solubility differences are more pronounced when the amount of hexavalent uranium present is significant. Under oxidizing atmosphere, more than 3.5 mol% UO_2 is readily incorporated into the aluminosilicate melt at 1400 °C, whereas the reduced species U^{V} and U^{IV} exhibit limited solubility between 1 and 2 mol% UO_2 (Fig. 3).

Regarding temperature, the solubility of an element generally increases with melting temperature [54]. In the case of a multivalent element such as uranium, an increase in temperature shifts the redox equilibrium toward the reduced species [1, 7, 55], thus exerting an opposite effect on solubility. Indeed, at a relatively high oxygen fugacity (around 10^{-6} atm), a U^{VI} fraction of approximately 30% is estimated in the glass A melted at 1250 °C. Raising the temperature to 1400 °C should reduce the amount of U^{VI} present, which may explain the lower solubility in the glass A prepared with the Ni/NiO buffer at 1400 °C in comparison to that at 1250 °C (AU4-NNO2 and AU4-NNO samples, respectively). Under a strongly reducing atmosphere, when U^{VI} content can be considered to be negligible relative to those of U^{V} and U^{IV}, the positive effect of temperature on the solubility of uranium seems to be more significant than the consequent changes in redox state. Under these highly reducing conditions, results show that higher temperatures allow greater uranium solubility in the glass melt. This result suggests that the solubilities of U^{V} and U^{IV} are quite similar. Unlike some scholars [1, 2], we assume here that uranium solubility in the glass melt is predominantly controlled by the U^{VI} content, rather than by the U^{IV} content. The presence or absence of hexavalent uranium will significantly change the total uranium content dissolved in the glass melt. Our data hint that U^{V}

is not significantly more soluble than U^{IV} in glass melts but rather that their solubilities are comparable. This is consistent with the fact that the structural environments of U^{V} and U^{IV} in silicate glasses are nearly identical [11]. Using EXAFS spectroscopy at the U L3 edge, the authors of previous work found a regular 6-coordinated site geometry for both oxidation states. The U^{IV}-O bond distances (2.26 - 2.29 Å) are slightly longer than the U^{V}-O bond distances (2.19–2.24 Å) which may be able to explain small variations in solubility.
The effect of the nature of the alkaline or earth alkaline element on the uranium solubility is not easy to evaluate. The basicities of glasses A and B after U-doping and MgO contamination are quite similar. The variations in sodium (volatilization) and calcium (crystallization) concentrations in our experiments do not allow for a conclusion to be reached. Results at 1400 °C show that melts A and B have very comparable U solubility limits under reducing conditions, except for at an oxygen fugacity of 10^{-6} atm. In that specific case, we assume that the oxidized species such as U^{VI} are favored by the composition of glass B, which would explain the increase in solubility observed between AU4-NNO2 and BU4-NNO2 samples. Based on literature data, it seems the uranium solubility in the silicate melt is affected more significantly by the amount of alkaline (or alkaline earth) element present than by the nature of alkaline element [9, 11].

In order to describe uranium solubility in glass melts, it appears to be necessary to know the distribution of uranium oxidation states, as many glass-making parameters affect the redox equilibria of U^{VI}-U^{V}-U^{IV}. Further experiments must be performed to confirm that the amount of hexavalent uranium effectively controls the uranium solubility. It would also be interesting to determine uranium solubility when only U^{VI} or U^{IV} species are present in the glass, and hence deduce the solubility of "pure" U^{V}. This would allow predictions of uranium solubility in glasses knowing the uranium oxidation state distribution, and vice versa. Besides, the study of effects of glass composition on the uranium solubility in the melt needs to be extended.

4.3 Comparison with data from the literature

To the authors' knowledge, there is very little data about uranium solubility in aluminosilicate glasses elaborated under reducing conditions reported in the literature. A solubility of 1 mol% UO_2 was announced in aluminosilicate melts containing mostly U^{IV} at 1240 °C under an oxygen fugacity of $10^{-12.8}$ atm [1]. This value is very close to the uranium solubility limit determined herein for the AU4-C soda-lime aluminosilicate glass, in which more than 75% of the total uranium was dissolved as the U^{IV} species in the glass matrix at 1250 °C. The same authors also reported a higher U^{IV} solubility in a borosilicate glass, about 2 mol% UO_2, at 1250 °C [2]. To explain this enhancement, the authors argued that borosilicate systems have a greater availability of sites for U^{IV} ions than aluminosilicate systems. An outstanding question concerns whether this is also the case for U^{V} and U^{VI} ions.

In order to prepare and optimize the production of radioactive glasses, surrogates (non-radioactive elements) that best simulate the properties of actinides are commonly used [54, 56, 57]. Therefore, it is worth comparing the behavior of uranium with that of its possible surrogates. As a multivalent species, uranium is not easy to simulate. Considering the redox conditions of our specific vitrification process (highly reducing conditions), uranium is expected to be mainly found in the U^{IV} oxidation state in the glass melt. In those conditions, hafnium has been identified as a potential surrogate for uranium [32]. It has a single oxidation state, tetravalent hafnium (Hf^{IV}). In addition, above the solubility limit, a precipitate separated from

the melt and principally composed of HfO_2 crystals was observed in hafnium-doped glasses. These high density HfO_2 and UO_2 crystals have the same tendency to settle at the bottom of the glass melt. In a previous study, the thermodynamic solubility of hafnium in the same aluminosilicate melts (glasses A and B) was determined [32]. The experiment protocol consisted of measuring the hafnium content in Hf-saturated glass in equilibrium with Hf-bearing crystals at different temperatures. The new set data for uranium, obtained under highly reducing conditions with U^{IV} as the main species, allows us to accurately compare the behavior of these two elements in a glass melt. Fig. 7 shows a comparison between the solubility limits of UO_2 and HfO_2 in the glasses A and B melted at 1250 and 1400 °C. Tetravalent hafnium is about three times more soluble than tetravalent uranium but similar trends are observed. For both, an increase in the melt temperature from 1250 to 1400 °C leads to a near doubling in the solubility. No profound effect is noticed upon the substitution of Na_2O with CaO. The comparison between hafnium and uranium deserves further investigation in the future.

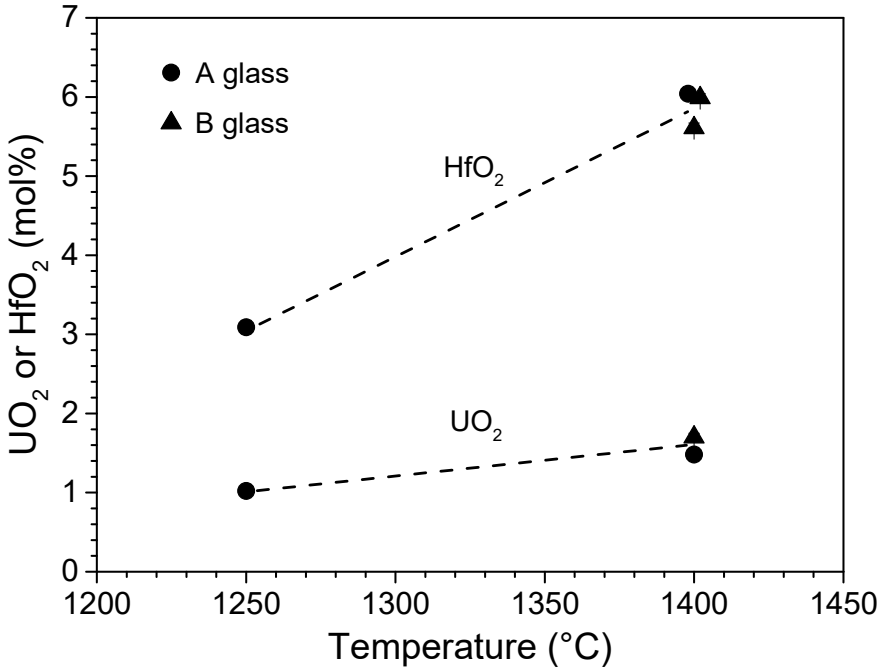

Fig. 7. Uranium and hafnium solubility limits versus temperature for several glass compositions. The symbols correspond to UO_2, and U-doped glasses were produced under strongly reducing conditions ($fO_2 < 10^{-12}$ atm). The data for HfO_2 are represented by open symbols and were published previously [32].The dashed lines are given simply as visual guides, and the random uncertainty is represented by error bars.

5 Conclusion

This study provides new insights into uranium solubility in reduced aluminosilicate glasses, which is relevant in the immobilization of nuclear waste. Taking advantage of the chemical properties of uranium, an original methodology is proposed for determination of the uranium solubility limit and speciation in Na-rich glass melts. The obtained data show that uranium solubility is clearly correlated with its three oxidation states, present simultaneously in the glass melt. The solubility decreases in the order $U^{VI} > U^{V} > U^{IV}$, although the solubilities of U^{V} and

U^{IV} seems to be quite similar. A structural approach might provide useful data in order to better understand this phenomenon. Uranium speciation is highly impacted by the oxygen fugacity, and also, albeit to a lesser extent, by the melting temperature and glass composition. The U M_4 edge HR-XANES method, which allows the determination of the distribution of the oxidation state of uranium, opens new methods for investigating uranium solubility in glasses. With this characterization technique, we demonstrate that tetravalent uranium is the main U valence present in an aluminosilicate glass melted under strongly reducing conditions, such as inside a graphite crucible. For the studied compositions, the solubility limit of U^{IV} in aluminosilicate glass is determined to 1 mol% UO_2 at 1250 °C, which can be enhanced to 1.5 mol% by increasing the temperature to 1400 °C. This new set of data for uranium has allowed its comparison with data for hafnium, which is a promising candidate for simulations of tetravalent uranium, as the two elements exhibit substantial similarities concerning their dissolution in glasses. It appears that tetravalent hafnium is much more soluble than tetravalent uranium in glass melts. Such differences deserve further investigation by a structural approach.

6 Acknowledgments

The authors gratefully acknowledge the synchrotron light source KARA for provision of instrumentation and beamtime. XAS experiments were supported by the TALISMAN project (grant agreement number 323300). The authors would also like to thank the Helmholtz Young Investigators Group (VH-NG-734) for setting up the HR-XANES measurement system. The authors are grateful to E. Gavilan and A. Caleyron from CEA Marcoule for their help with the preparation of some uranium-doped glasses. The authors thank the SEM team (C. David and E. Excoffier) for access to equipment in a controlled area. Finally, the author acknowledge the reviewers for their valuable suggestions. This research was funded by the French Alternative Energies and Atomic Energy Commission (CEA), Orano, and within the Investments for the Future Program of the French Government and operated by the French National Radioactive Waste Management Agency (Andra).

7 References

[1] H.D. Schreiber, The Chemistry of Uranium in Glass-Forming Aluminosilicate Melts, Journal of the Less-Common Metals 91(1) (1983) 129-147.

[2] H.D. Schreiber, G.B. Balazs, The Chemistry of Uranium in Borosilicate Glasses .1. Simple Base Compositions Relevant to the Immobilization of Nuclear Waste, Phys. Chem. Glasses 23(5) (1982) 139-146.

[3] H.D. Schreiber, G.B. Balazs, B.J. Williams, The Chemistry of Uranium in Synthetic Silicate Liquids, Lunar and Planetary Science Conference (1981).

[4] G. Calas, Experimental-Study of Behavior of Uranium in Magmas - Oxidation-States and Coordination, Geochim. Cosmochim. Acta 43(9) (1979) 1521-1531.

[5] C.D. Wirkus, D.R. Wilder, Uranium-Bearing Glasses in the Silicate and Phosphate Systems, J. Nucl. Mater. 5(1) (1962) 140-146.

[6] S. Bahl, S. Peuget, I. Pidchenko, T. Pruessmann, J. Rothe, K. Dardenne, J. Delrieu, D. Fellhauer, C. Jégou, H. Geckeis, T. Vitova, Pu Coexists in Three Oxidation States in a Borosilicate Glass: Implications for Pu Solubility, Inorg. Chem. 56(22) (2017) 13982-13990.

[7] J.N. Cachia, X. Deschanels, C. Den Auwer, O. Pinet, J. Phalippou, C. Hennig, A. Scheinost, Enhancing cerium and plutonium solubility by reduction in borosilicate glass, J. Nucl. Mater. 352(1-3) (2006) 182-189.

[8] G.S. Knapp, B.W. Veal, A.P. Paulikas, A.W. Mitchell, D.J. Lam, T.E. Klippert, EXAFS Studies of Sodium Silicate Glasses Containing Dissolved Actinides, Springer Proceedings in Physics, Berlin ,Heidelberg, 1984, pp. 305-307.
[9] F. Domine, B. Velde, Preliminary Investigation of the Processes Governing the Solubility of Uranium in Silicate Melts, Bulletin De Mineralogie 108(6) (1985) 755-765.
[10] D.J. Lam, B.W. Veal, A.P. Paulikas, X-Ray Photoemission Spectroscopy (Xps) Study of Uranium, Neptunium, and Plutonium Oxides in Silicate-Based Glasses, Acs Symposium Series 216 (1983) 145-154.
[11] F. Farges, C.W. Ponader, G. Calas, G.E. Brown, Structural Environments of Incompatible Elements in Silicate Glass Melt Systems .2. Uiv, Uv, and Uvi, Geochim. Cosmochim. Acta 56(12) (1992) 4205-4220.
[12] G.S. Knapp, B.W. Veal, D.J. Lam, A.P. Paulikas, H.K. Pan, EXAFS studies of silicate glasses containing uranium, Materials Letters 2(4, Part A) (1984) 253-256.
[13] D. Petit-Maire, J. Petiau, G. Calas, N. Jacquet-Francillon, Local Structure around Actinides in Borosilicate Glasses, Journal De Physique 47(C-8) (1986) 317-320.
[14] S.V. Stefanovsky, A.A. Shiryaev, J.V. Zubavitchus, A.A. Veligjanin, J.C. Marra, Valence state and speciation of uranium ions in borosilicate glasses with a high iron and aluminum content, Glass Phys. Chem. 35(2) (2009) 141-148.
[15] S.V. Stefanovsky, O.I. Stefanovskaya, V.Y. Murzin, A.A. Shiryaev, B.F. Myasoedov, Oxidation state and coordination environment of uranium in sodium iron aluminophosphate glasses, Dokl. Phys. Chem. 468 (2016) 76-79.
[16] J.A. Duffy, Optical basicity: A practical acid-base theory for oxides and oxyanions, J. Chem. Educ. 73(12) (1996) 1138-1142.
[17] H.D. Schreiber, B.K. Kochanowski, C.W. Schreiber, A.B. Morgan, M.T. Coolbaugh, T.G. Dunlap, Compositional Dependence of Redox Equilibria in Sodium-Silicate Glasses, Journal of Non-Crystalline Solids 177 (1994) 340-346.
[18] M.A. Carrell, D.R. Wilder, Visible and near-Infrared Absorption of Uranium in Sodium-Silicate Glass, J. Nucl. Mater. 13(2) (1964) 142-151.
[19] D.G. Karraker, Actinide Valences in Borosilicate Glass, J. Am. Ceram. Soc. 65(1) (1982) 53-55.
[20] P.G. Eller, G.D. Jarvinen, J.D. Purson, R.A. Penneman, R.R. Ryan, F.W. Lytle, R.B. Greegor, Actinide Valences in Borosilicate Glass, Radiochim. Acta 39(1) (1985) 17-22.
[21] G.N. Greaves, N.T. Barrett, G.M. Antonini, F.R. Thornley, B.T.M. Willis, A. Steel, Glancing-Angle X-Ray Absorption-Spectroscopy of Corroded Borosilicate Glass Surfaces Containing Uranium, J. Am. Chem. Soc. 111(12) (1989) 4313-4324.
[22] J.I. Pacold, W.W. Lukens, C.H. Booth, D.K. Shuh, K.B. Knight, G.R. Eppich, K.S. Holliday, Chemical speciation of U, Fe, and Pu in melt glass from nuclear weapons testing, J. Appl. Phys. 119(19) (2016).
[23] Y. Matyunin, S. Yudintsev, Y. Dikov, Characterization of U-containing borosilicate glass gp91 with X-ray photoelectron spectroscopy, WM'00 Conference, Tuscon, AZ (2000).
[24] T. Vitova, K.O. Kvashnina, G. Nocton, G. Sukharina, M.A. Denecke, S.M. Butorin, M. Mazzanti, R. Caciuffo, A. Soldatov, T. Behrends, H. Geckeis, High energy resolution x-ray absorption spectroscopy study of uranium in varying valence states, Phys. Rev. B 82(23) (2010).
[25] R. Bes, M. Rivenet, P.L. Solari, K.O. Kvashnina, A.C. Scheinost, P.M. Martin, Use of HERFD-XANES at the U L-3- and M-4-Edges To Determine the Uranium Valence State on [Ni(H2O)(4)](3)[U(OH,H2O)(UO2)(8)O-12(OH)(3)], Inorg. Chem. 55(9) (2016) 4260-4270.
[26] K.O. Kvashnina, S.M. Butorin, P. Martin, P. Glatzel, Chemical State of Complex Uranium Oxides, Phys. Rev. Lett. 111(25) (2013).
[27] G. Leinders, R. Bes, J. Pakarinen, K. Kvashnina, M. Verwerft, Evolution of the Uranium Chemical State in Mixed-Valence Oxides, Inorg. Chem. 56(12) (2017) 6784-6787.
[28] I. Pidchenko, K.O. Kvashnina, T. Yokosawa, N. Finck, S. Bahl, D. Schild, R. Polly, E. Bohnert, A. Rossberg, J. Gottlicher, K. Dardenne, J. Rothe, T. Schafer, H. Geckeis, T. Vitova, Uranium Redox Transformations after U(VI) Coprecipitation with Magnetite Nanoparticles, Environ. Sci. Technol. 51(4) (2017) 2217-2225.

[29] K. Popa, D. Prieur, D. Manara, M. Naji, J.F. Vigier, P.M. Martin, O.D. Blanco, A.C. Scheinost, T. Prussmann, T. Vitova, P.E. Raison, J. Somers, R.J.M. Konings, Further insights into the chemistry of the Bi-U-O system, Dalton Trans. 45(18) (2016) 7847-7855.
[30] A.L. Smith, P.E. Raison, L. Martel, D. Prieur, T. Charpentier, G. Wallez, E. Suard, A.C. Scheinost, C. Hennig, P. Martin, K.O. Kvashnina, A.K. Cheetham, R.J.M. Konings, A New Look at the Structural Properties of Trisodium Uranate Na3UO4, Inorg. Chem. 54(7) (2015) 3552-3561.
[31] T. Vitova, I. Pidchenko, S. Biswas, G. Beridze, P.W. Dunne, D. Schild, Z.M. Wang, P.M. Kowalski, R.J. Baker, Dehydration of the Uranyl Peroxide Studtite, [UO2(eta(2)-O-2)(H2O)(2)]center dot 2H(2)O, Affords a Drastic Change in the Electronic Structure: A Combined X-ray Spectroscopic and Theoretical Analysis, Inorg. Chem. 57(4) (2018) 1735-1743.
[32] P. Chevreux, A. Laplace, E. Deloule, L. Tissandier, N. Massoni, Hafnium solubility determination in soda-lime aluminosilicate glass, Journal of Non-Crystalline Solids 457 (2017) 13-24.
[33] A. Tsuchiyama, H. Nagahara, I. Kushiro, Volatilization of Sodium from Silicate Melt Spheres and Its Application to the Formation of Chondrules, Geochim. Cosmochim. Acta 45(8) (1981) 1357-1367.
[34] L.S. Walter, Giutroni.Je, Vapor Fractionation of Silicate Melts at High Temperatures and Atmospheric Pressures, Sol. Energy 11(3-4) (1967) 163-169.
[35] T.K. Abdullah, C. Petitjean, P.J. Panteix, C. Rapin, M. Vilasi, Z. Hussain, A.A. Rahim, Dissolution equilibrium of chromium oxide in a soda lime silicate melt exposed to oxidizing and reducing atmospheres, Mater. Chem. Phys. 142(2-3) (2013) 572-579.
[36] H. Khedim, R. Podor, C. Rapin, M. Vilasi, Redox-Control Solubility of Chromium Oxide in Soda-Silicate Melts, J. Am. Ceram. Soc. 91(11) (2008) 3571-3579.
[37] R. Mathieu, H. Khedim, G. Libourel, R. Podor, L. Tissandier, E. Deloule, F. Faure, C. Rapin, M. Vilasi, Control of alkali-metal oxide activity in molten silicates, Journal of Non-Crystalline Solids 354(45-46) (2008) 5079-5083.
[38] E. Schmucker, C. Petitjean, L. Martinelli, P.J. Panteix, S. Ben Lagha, M. Vilasi, Oxidation of Ni-Cr alloy at intermediate oxygen pressures. I. Diffusion mechanisms through the oxide layer, Corrosion Sci. 111 (2016) 474-485.
[39] X. Feng, H. Li, L.L. Davis, L. Li, J.G. Darab, M.J. Schweiger, J.D. Vienna, B.C. Bunker, P.G. Allen, J.J. Bucher, I.M. Craig, N.M. Edelstein, D.K. Shuh, R.C. Ewing, L.M. Wang, E.R. Vance, Distribution and solubility of radionuclides in waste forms for disposition of plutonium and spent nuclear fuels: Preliminary results, Environmental Issues and Waste Management Technologies in the Ceramic and Nuclear Industries Iv, Amer Ceramic Soc, Westerville (1999) 409-419.
[40] C.H. Donaldson, R.J. Williams, G. Lofgren, Sample Holding Technique for Study of Crystal-Growth in Silicate Melts, Am. Miner. 60(3-4) (1975) 324-326.
[41] D.C. Presnall, N.L. Brenner, Method for Studying Iron Silicate Liquids under Reducing Conditions with Negligible Iron Loss, Geochim. Cosmochim. Acta 38(12) (1974) 1785-1788.
[42] A. Zimina, K. Dardenne, M.A. Denecke, D.E. Doronkin, E. Huttel, H. Lichtenberg, S. Mangold, T. Pruessmann, J. Rothe, T. Spangenberg, R. Steininger, T. Vitova, H. Geckeis, J.D. Grunwaldt, CAT-ACT-A new highly versatile x-ray spectroscopy beamline for catalysis and radionuclide science at the KIT synchrotron light facility ANKA, Rev. Sci. Instrum. 88(11) (2017).
[43] V.A. Solé, E. Papillon, M. Cotte, P. Walter, J. Susini, A multiplatform code for the analysis of energy-dispersive X-ray fluorescence spectra, Spectrochimica Acta Part B: Atomic Spectroscopy 62(1) (2007) 63-68.
[44] B. Ravel, M. Newville, ATHENA, ARTEMIS, HEPHAESTUS: data analysis for X-ray absorption spectroscopy using IFEFFIT, Journal of Synchrotron Radiation 12(4) (2005) 537-541.
[45] H.A. Schaeffer, T. Frey, I. Loh, F.G.K. Baucke, Oxidation-State of Equilibrated and Non-Equilibrated Glass Melts, Journal of Non-Crystalline Solids 49(1-3) (1982) 179-188.

[46] F.G.K. Baucke, High-temperature oxygen sensors for glass-forming melts, Fresenius J. Anal. Chem. 356(3-4) (1996) 209-214.
[47] J. Holc, D. Kolar, Reinvestigation of Phase-Relations in the Cao-Uo2 System, J. Solid State Chem. 61(2) (1986) 260-262.
[48] Y. Podkovyrina, I. Pidchenko, T. Prussmann, S. Bahl, J. Goettlicher, A. Soldatov, T. Vitova, Probing Covalency in the UO3 Polymorphs by U M-4 edge HR-XANES, Journal of Physics Conference Series 712 (2016) 012092.
[49] T. Vitova, J.C. Green, R.G. Denning, M. Loble, K. Kvashnina, J.J. Kas, K. Jorissen, J.J. Rehr, T. Malcherek, M.A. Denecke, Polarization Dependent High Energy Resolution X-ray Absorption Study of Dicesium Uranyl Tetrachloride, Inorg. Chem. 54(1) (2015) 174-182.
[50] T. Vitova, M. Denecke, J. Goettlicher, K. Jorissen, J. Kas, K. Kvashnina, T. PrüBmann, J. Rehr, J. Rothe, Actinide and lanthanide speciation with high-energy resolution X-ray techniques, Journal of Physics Conference Series 430 (2013) 2117.
[51] F.L. Binsbergen, Heterogeneous nucleation of crystallization, Progress in Solid State Chemistry 8 (1973) 189-238.
[52] P.W. Voorhees, The Theory of Ostwald Ripening, J. Stat. Phys. 38(1-2) (1985) 231-252.
[53] J.H. Yao, K.R. Elder, H. Guo, M. Grant, Theory and Simulation of Ostwald Ripening, Phys. Rev. B 47(21) (1993) 14110-14125.
[54] X. Deschanels, S. Peuget, J.N. Cachia, T. Charpentier, Plutonium solubility and self-irradiation effects in borosilicate glass, Prog. Nucl. Energy 49(8) (2007) 623-634.
[55] H. Khedim, T. Katrina, R. Podor, P.J. Panteix, C. Rapin, M. Vilasi, Solubility of Cr2O3 and Speciation of Chromium in Soda-Lime-Silicate Melts, J. Am. Ceram. Soc. 93(5) (2010) 1347-1354.
[56] L.L. Davis, J.G. Darab, M. Qian, D. Zhao, C.S. Palenik, H. Li, D.M. Strachan, L. Li, Hafnium in peralkaline and peraluminous boro-aluminosilicate glass and glass sub-components: a solubility study, Journal of Non-Crystalline Solids 328(1-3) (2003) 102-122.
[57] C. Lopez, X. Deschanels, C. Den Auwer, J.N. Cachia, S. Peuget, J.M. Bart, X-ray absorption studies of borosilicate glasses containing dissolved actinides or surrogates, Phys. Scr. T115 (2005) 342-345.